



Investigation the catalytic profile of Eu and Pr doped CeO₂ nanoparticles for the thermal behavior of AP

Jalpa A. Vara¹ · Pragnesh N. Dave^{1,2}

© Springer Nature Switzerland AG 2019

Abstract

In these studies we report the catalytic proficiency of two Eu and Pr doped CeO₂ nanoparticles on the thermal behaviour of powder AP and CSPs samples. A co-precipitation method was used for synthesizing Eu and Pr doped CeO₂ nanoparticles and they were characterized by XRD, FTIR, and SEM with EDX. The catalytic proficiency of both Eu and Pr doped CeO₂ nanoparticles were investigated by utilizing TG–DSC technique. The FWO, KAS, and Starink methods were used to determine activation energies of all catalyzed AP and CSPs samples. The catalytic proficiency increased by addition of Eu and Pr doped CeO₂ nanoparticles and decomposition temperature decreased in the presence of catalyst. The activation energy decreased by the addition of Eu and Pr doped CeO₂ nanoparticles in AP and CSPs, the burning rate of CSPs found to increase by the addition of Eu and Pr doped CeO₂ nanoparticles. The Pr doped CeO₂ nanoparticles showed good catalytic efficiency on AP and CSPs that reduced the decomposition temperature around 70 °C for AP and 20 °C for CSPs. The activation energy of CSPs catalyzed by Pr doped CeO₂ nanoparticles reported 150.12, 147.60, and 146.83 kJ mol⁻¹ by FWO, KAS, and Starink method respectively which decreases in existence of catalyst in CSPs.

Keywords Ammonium perchlorate (AP) · Catalytic proficiency · Nanoparticles · Activation energy · Burning rate

1 Introduction

The ammonium perchlorate (AP) based propellants and their perchlorate explosives are less responsive to commotion and environmental changes than dynamite. Due to these properties they gained intense attention from the researchers. In addition, they have applications in the diverse field [1, 2]. The AP has defined role in the fields like military and aerospace [3–5]. As constitute in the composite solid propellants (CSPs), role of AP is vital and main oxidizing agents. It has a vast influence over the burning performance [1–5] of CSPs. The production of huge amount of burning gases from propellants especially associated with its burning rate with curtailed time and it is necessary to empower rockets to take off at faster speeds. The chemical stability and slow decomposing profile at lower temperature makes them suitable composite to elicit

the better or improve the decomposition traits of AP to meet the demand of generate high energy at low temperature. Therefore, The effect of AP on the on the ignited rate of solid propellant have been established by several researches [6–8].

Lanthanide including rare earth elements have brought more interest in academic research and industry, by reason their uncommon physical and chemical properties [9]. Lanthanide elements have a huge application, because of their crucial role for a number of demanding technologies [10]. Rare metals are possessing exclusive magnetic and optical properties related through their *f*-electronic configurations [11].

In the redox reactions, the cerium oxides claim as an integral part because of it owing the multivalent oxidation states with movable oxygen species. The fact is renowned in our venture to establish high temperature stable profile of

✉ Pragnesh N. Dave, pragneshdave@gmail.com | ¹Department of Chemistry, K S K V Kachchh University, Mundra Road, Bhuj, Gujarat 370 001, India. ²Department of Chemistry, Sardar Patel University, Vallabh Vidyangar, Gujarat 388 120, India.



burning rate enhancer for the decomposition of energetic oxidizer like AP. The cerium oxide considered as one of well famous heterogeneous catalyst and it has a characteristic to alter the nature of catalyst in three ways. The self-adjusting ability makes them suitable in combination with previously known noble metals. The doping of cerium oxide with other metal provides the synergistic effect that is well famous in the territory of catalysis. The proficiency of cerium is to form non-stoichiometric matrix with dopants and it is also able to alter the reaction routes [12–16]. In addition, the cerium changes between Ce^{4+} and Ce^{3+} with ease. Further, high mobility, storage capacity of oxygen within the lattice and profusion of cerium on the planet like properties makes them alternative to noble metal.

Since ceria can become non-stoichiometric in the presence of dopants in its matrix and alter reaction routes [12–16]. The doping is crucial technique to enhance the proficiency of cerium as a catalyst. In doping, two techniques employ to enhance the proficiency. First, the abstraction of cerium accomplish by partial substitution of cerium by other cations in its crystal lattice. The second way, to develop the nanocrystals with generation of surface crystal defects [17, 18]. The utility of nanofabrication techniques employ to assist over the selectivity and the activity of oxide catalysts.

The nano-size materials attained extreme research interest as a consequence to their size effect, electronic, optical characteristics, the role-played by surface phenomena as the reduced size and doped nanomaterials have additional synergistic profound effect. The metal in oxide form of nanoparticles has exceptional characteristics and their applications have been contemplated vast fields like chemistry, photonics, biomedicine, and electronics [19–22]. The AP is surprisingly responsive to additives of metal oxide, especially nanomaterial i.e. thermal decomposition trait of oxidizer (AP) will effect on burning performance of the CSPs [23–26].

In this paper, to investigate the catalytic role of Eu and Pr doped CeO_2 nanoparticles in AP and CSPs, a Eu and Pr doped CeO_2 nanoparticles were prepared by a co-precipitation method. The catalytic proficiency of Eu and Pr doped CeO_2 nanoparticles on the thermal decomposition of AP and CSPs was investigated by TG–DSC techniques. The activation energies of catalyzed AP and CSPs were also evaluated by Starink, KAS and FWO. Further investigation found that Eu and Pr doped CeO_2 nanoparticles promote the decomposition of AP.

2 Experimental

2.1 Reagents and chemicals

All metal nitrates were acquired from CDH. NaOH was acquired from Merck and Hydroxyl-terminated

polybutadiene (HTPB), IPDI (Isophorone di isocyanate), Di Octyle Adipate (DOA) and AP was acquired from National chemicals.

2.2 Synthesis of nanoparticles

The synthesis for Eu and Pr doped CeO_2 nanoparticles executed by chemical co-precipitation procedure reported elsewhere [27]. 0.1 M nitrate solution of A (here A = Eu and Pr) and 0.2 M solution of cerium nitrate obtained by addition of appropriate quantity of water and mixed it. The 0.5 M NaOH used as alkali media and dropwise addition required to offer the alkali environment for to accomplish the metal hydroxide precipitation with continue stirring. A metal hydroxides precipitation was occurred at pH 11–12 and then precipitate washed with water to prepare nanoparticles and keep them free from nitrate ions. The brown metal hydroxide was dried at 60 °C in an oven for 5 h and then it was calcined at 300 °C for 5 h.

2.3 Characterization

The characterization of all nanoparticles was done by utilizing X-ray Diffraction (Rigaku, mini flex 600) with CuK α radiation ($\lambda = 1.5418$) and FTIR spectrum were investigated by MB 3000 FTIR spectrometer (ABB Pvt. Ltd., Germany) with ATR (horizontal attenuated total reflection). The morphology of Eu and Pr doped CeO_2 nanoparticles was studied by utilizing Scanning Electronic Microscopy (SEM, JEOL JSM-6510 LV) with 25 kV voltages. The crystalline size of nanoparticles could be obtained by implementation of Scherrer's equation [28].

2.4 Preparation of CSPs

The preparation of CSPs was mixing of AP and nano-catalyst in 3:1 ratio. This mixture was added in the HTPB of the 3:1 proportion. Then 20% of IPDI curing agent was added in the same proportion to HTPB and 30% DOA as a plasticizer to HTPB. The mixture was mixed for 1 h at 60 °C. Then this mixture was casted into aluminum plates includes dimensions of $1 \times 3 \times 10 \text{ cm}^3$ and it was kept in an oven for 10–15 days at 70 °C [29, 30].

2.4.1 Measurement of burning rate

The propellant samples were cut into small portion including dimensions of $0.8 \times 0.8 \times 9.0 \text{ cm}^3$ and the burning rate was reliable at ambient pressure through fuse wire technique [30]. An average of three assessments was taken.

2.5 Thermal analysis

Thermal analysis of AP with and without adding Eu and Pr doped CeO₂ nanoparticles were measured by utilizing a TG–DSC of Perkin Elmer STA-8000 instrument. The samples were noted down 12 mg by 99:1 ratio of AP with and without Eu and Pr doped CeO₂ nanoparticles in N₂ atmosphere (20 ml/min) at 10 °C min⁻¹ heating rate by using platinum crucible. AP based CSPs with and without adding Eu and Pr doped CeO₂ nanoparticles was measured by utilizing a TG–DSC of TA Instruments SDT Q600, and all CSPs samples were noted down 20 mg samples in N₂ atmosphere (100 ml/min) at 10 °C min⁻¹ heating rate with using alumina crucible.

2.6 Kinetic studies

The three heating rate at 5, 10, and 15 °C min⁻¹ was induced in the DSC investigation. The assessment activation energy has been calculated by Flynn–wall–Ozawa (FWO), Kissinger–akahira–sunose (KAS), and Starink methods [31–33]. Ozawa, Kissinger and Starink methods based on Eqs. 1, 2 and 3, respectively. The activation energy is predicted from the value of slope of a graphs lnβ for FWO, lnβ/T² for KAS and lnβ/T^{1.92} for Starink against 1000/T. A series of studies performed with different heating (β), where T_m is the peak temperature of the DSC thermogram.

$$\ln(\beta) = \ln\left(\frac{A \cdot E_a}{R}\right) - 5.331 - 1.0516 \frac{E_a}{RT_m} \quad (1)$$

$$\ln\left(\frac{\beta}{T_m^2}\right) = \ln\left(\frac{AR}{E_a}\right) - \frac{E_a}{RT_m} \quad (2)$$

$$\ln\left(\frac{\beta}{T_m^{1.92}}\right) = \ln\left(\frac{AR^{0.92}}{E_a^{0.92}}\right) - 0.312 - 1.0008 \frac{E_a}{RT_m} \quad (3)$$

The values of activation energy (E_a) and the exponential factor (A) can be calculated from the value of slope and the intercept respectively.

3 Results and discussion

3.1 Characterization of nanoparticles

The Fig. 1 demonstrates the XRD pattern of CeO₂ systems with doped Eu and Pr. The XRD diffractogram of all the powder form samples of Eu and Pr doped CeO₂ systems are in concur with the face centered cubic structure of CeO₂

(JCPDS NO. 34-0394). While considering the XRD patterns, the Eu and Pr doped CeO₂ samples demonstrated without the forming of secondary phase. The XRD diffractogram of doped CeO₂ peaks stating to lattice planes of fcc and abatement noticed in the crystallinity of Eu and Pr doped CeO₂ after inclusion of Pr³⁺ and Eu³⁺ ions in the oxide lattice. The Eu³⁺ and Pr³⁺ ions acquire the larger ionic radii 0.1066 nm and 0.1126 nm in contrast to Ce⁴⁺ (0.0970 nm). While these ions inserted in the CeO₂ lattice that, swap the Ce⁴⁺ ions. Therefore, the deviation in peak position (2θ) at lower angle noticed which inferring after the swapping of Eu and Pr in CeO₂ lattice [34]. The formation of oxygen vacancies in the cerium crystal structure can be efficient by exchange of Ce⁴⁺ ions by Eu³⁺ and Pr³⁺ ions in CeO₂ systems [35]. Further, the reduction in the crystallite size can be prophesied by the event of broadening peaks in patterns. The assessment of average crystalline size of Eu and Pr doped CeO₂ nanoparticles were evaluated by Scherrer formula [28, 36, 37]. The crystalline size of Eu and Pr doped CeO₂ nanoparticles is 5.02 and 4.40 nm respectively. These results are concurs with reported studies [38, 39].

Figure 2 demonstrates the FT-IR spectra of Eu and Pr doped CeO₂ nanoparticles. The appearance of two strong intense bands detected at 3400 and 1650 cm⁻¹ in the spectrum of Eu doped CeO₂ are imputed to stretching and bending vibration modes of O–H. Further, the spectra of Pr doped CeO₂ showed 3418 and 1652 cm⁻¹ of two bands are imputed to stretching and bending vibration modes of O–H group. The bands are noticed because of the existence of water on the samples observed physically

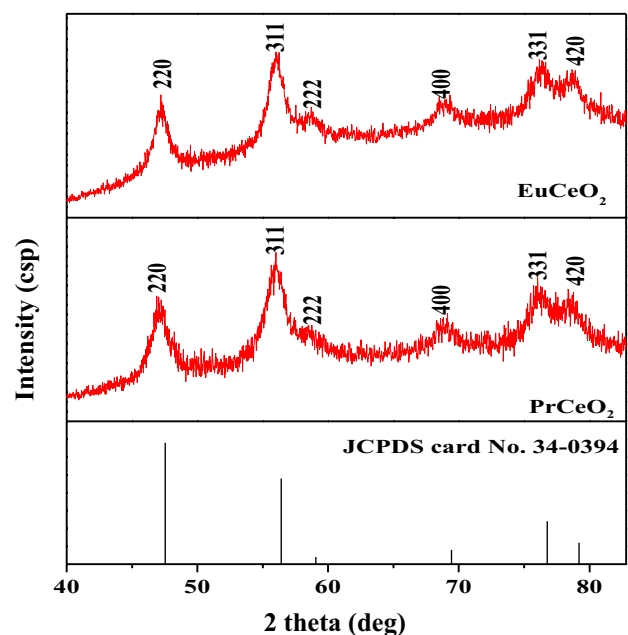


Fig. 1 XRD diffractogram of Eu and Pr doped CeO₂ nanoparticles

[40, 41]. The values of bands observed for stretching and bending vibration modes of O–H were slightly higher for Pr doped CeO₂ in contrast to Eu doped CeO₂ nanoparticles. The advent of new band 879 cm⁻¹ in the spectrum of Eu doped CeO₂ and 887 cm⁻¹ in the spectrum Pr doped CeO₂ noticed and which indicated the lower double bond nature between the Ce–O–Ce group. The advent of new band 710 cm⁻¹ in the spectrum of Eu doped CeO₂ and 720 cm⁻¹ in the spectrum Pr doped CeO₂ noticed and corresponding to the Ce–O–Ce chains asymmetric stretching vibration of metal oxide networks. The doping of CeO₂ by Eu and Pr confirmed by arrival of new two bands at 620 and 606 cm⁻¹ detected for Eu doped CeO₂ and Pr doped CeO₂ nanoparticles. The two bands appearance at 620 and 606 cm⁻¹ inferred the symmetrical stretching vibration mode of (Ce–O–Ce) or (Ce–O–Eu) and (Ce–O–Pr). [42] In addition, doping of Eu and Pr changed the length of the M–O bond. These shifts in bands confirm the consolidation of dopant in parent lattice [43].

The morphology segment of nanoparticles was evaluated by utilizing the SEM. SEM image of Eu and Pr doped CeO₂ nanoparticles prepared via co-precipitation are shown in Fig. 3. The SEM image show the Eu and Pr doped CeO₂ nanoparticles consist of agglomerated particles and polygonal shape of Eu and Pr doped CeO₂ nanoparticles. The SEM image of the annealed Eu and Pr doped CeO₂ nanoparticles at 300 °C for 5 h demonstrates in the Fig. 3a and b. The image for Eu and Pr doped CeO₂ nanoparticles (Fig. 3) manifests the as synthesized nanoparticles with reasonably uniform size distribution with some unspecified reason larger size than that of the grain size obtained from XRD analysis. This could be indicant for the formation of secondary particles by aggregation of the primary

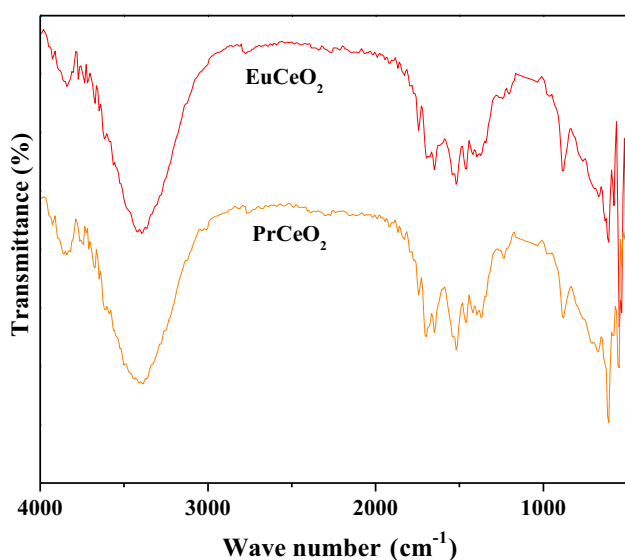


Fig. 2 FTIR graph of Eu and Pr doped CeO₂ nanoparticles

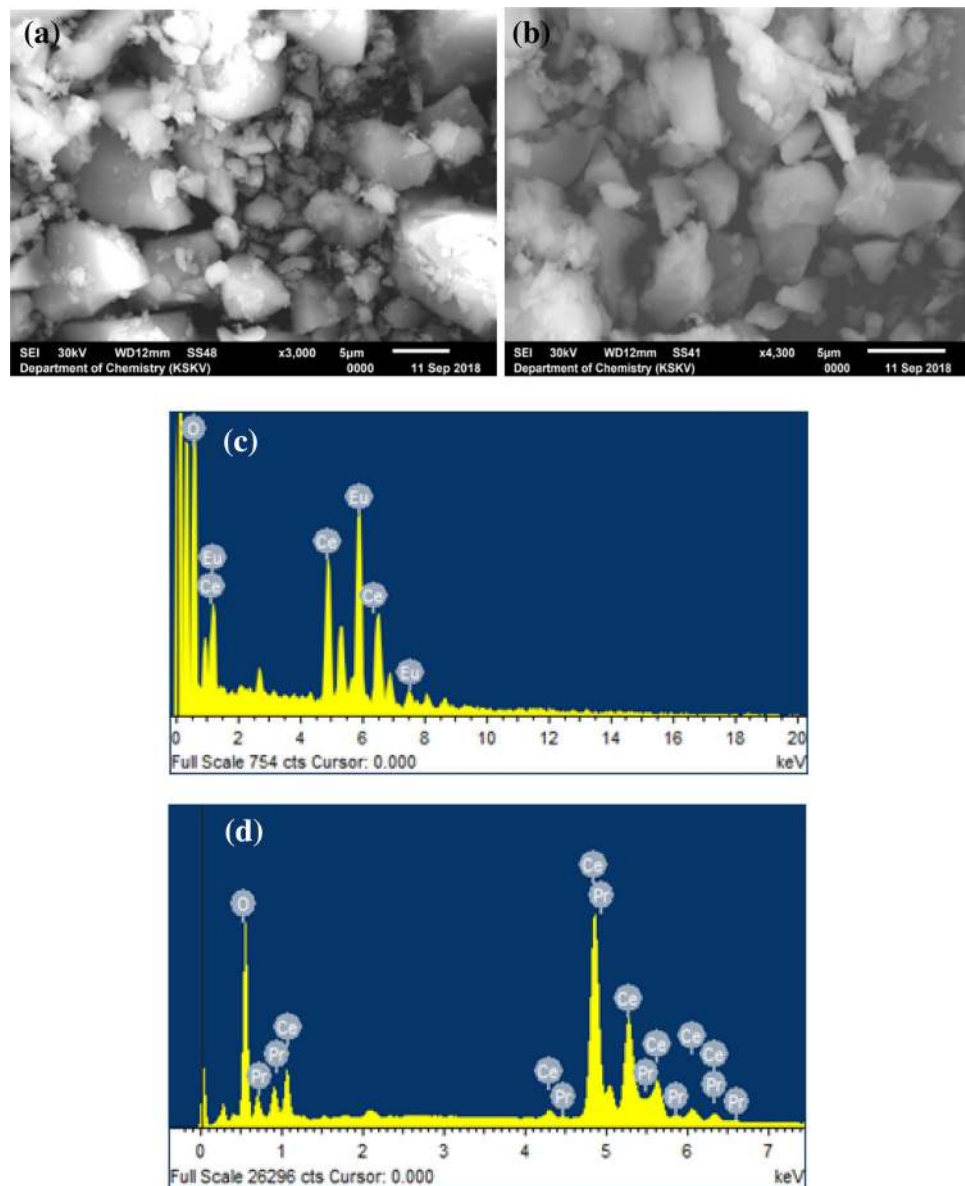
particles. For the Eu and Pr doped ZnO samples, the particles seem to be more and more agglomerated, and consequently it is hard to say with greater degree about the grain size obtained from the less-resolved SEM images (Fig. 3) [44]. EDX was applied to Eu and Pr doped CeO₂ nanoparticles prepared by co precipitation revealed in Fig. 3c and d. The EDX spectra are acquired at low magnification of the powders shown in Fig. 3c and d. EDX of these prepared Eu and Pr doped CeO₂ nanoparticles shows that they are pure nanoparticles containing Eu or Pr and Ce.

3.2 The catalytic proficiency of nanoparticles on AP

The AP with 1 wt % of Eu and Pr doped CeO₂ nanoparticles was used to explore the thermal enactment at 10 °C min⁻¹ heating rates by using Perkin Elmer STA 8000 instrument. The pure AP also executed with same condition to evaluate the catalytic proficiency of doped nanoparticle systems. In TG thermograms, Fig. 4a reveals the two-stages mass loss of pure AP at 285–425 °C temperature range. These types of results are also reported for mass loss of pure AP [45–47]. In first stage segment, 16% mass loss of pure AP delivered between 285 and 350 °C of temperature range which coincides with the conversion of AP into intermediate products such as NH₃ and HClO₄. In the second stage, 80% of mass loss perceived at 350–425 °C of higher temperature with complete decomposition of AP. The complete decomposition of AP was rationalized by release of volatile product. The results of TG thermogram are well coordinated with the derivative thermogravimetry (DTG) data shown in Fig. 4b for pure AP with two endothermic peaks was appeared around 307.02 and 390.11 °C. Increased endothermic heat requirement in between the two exothermic peaks appears as a shoulder in the TG graph [48]. While considering TG thermogram of 1 wt% Eu doped CeO₂ nanoparticles added with AP in the Fig. 4a, it revealed one step mass loss stage with 99.52% of Eu doped CeO₂ nanoparticles with AP and the decomposition temperature shifted from 285 to 362 °C for it. In addition, TG thermogram of Pr doped CeO₂ nanoparticles with AP in Fig. 4a established one step mass loss with 98.75% and decomposition temperature shifted from 285 to 347 °C for it. From TG thermogram in Fig. 4a for the Eu and Pr doped CeO₂ nanoparticles depicted that doped CeO₂ nanoparticles have a catalytic accomplishment over the AP thermal response. The catalytic proficiency of Eu and Pr doped CeO₂ nanoparticles have been entrenched by one stage decomposition at a lower temperature of quick oxidation of the AP.

Thermal decomposition of energetic oxidizer (AP) was fascinated by DSC technique. In Fig. 5a, exposes DSC thermogram of pure AP with one endothermic peak and two exothermic peaks. The one endothermic peak detected at

Fig. 3 **a** SEM images and **b** EDX spectra for **c** EuCeO_2 , **d** PrCeO_2 nanoparticles



243.12 °C that recognized as the crystal structural transition from orthorhombic to cubic [49]. The one exothermic peak for the cubic form arrive at 310.30 °C denotes the partial extinction of AP at lower temperature decomposition and another exothermic decomposition peak noticed at 395.12 °C denotes the complete AP decomposition at high-temperature decomposition. In DSC curves, the necessary increment in the endothermic heat obligation among the two exothermic peaks which fascinated the occurrence of endothermic incident instantly prior to second exothermic decomposition peak of AP [48]. Inclusive, two steps of post transition decomposition compartment observed for AP and it is good agreement with TG and DSC data of AP reported previously [25, 50–53] and the endothermic peak noticed in good agreement. The TG

decomposition pattern of AP within corporation of Eu and Pr doped CeO_2 nanoparticles. The TG graphs quite differ in contrast to pure AP. The changes are observed which recognized the catalytic trait of doped CeO_2 nanoparticles. While the deal with DSC curves, there is no deviation observed in the endothermic peak for Eu and Pr doped CeO_2 nanoparticles with AP in compare to pure AP. Further, the one intense exothermic peak arose at 340.44, and 326.89 °C for both Eu and Pr doped CeO_2 nanoparticles at the lower temperature of AP revealed in Table 1. The DTA data in Fig. 5b are also compatible with DSC data. The catalytic proficiency of Eu and Pr doped CeO_2 nanoparticles on the decomposition of AP understood by reducing the decomposition temperature correlate to pure AP. The Eu and Pr doped CeO_2 nanoparticles with AP are efficient

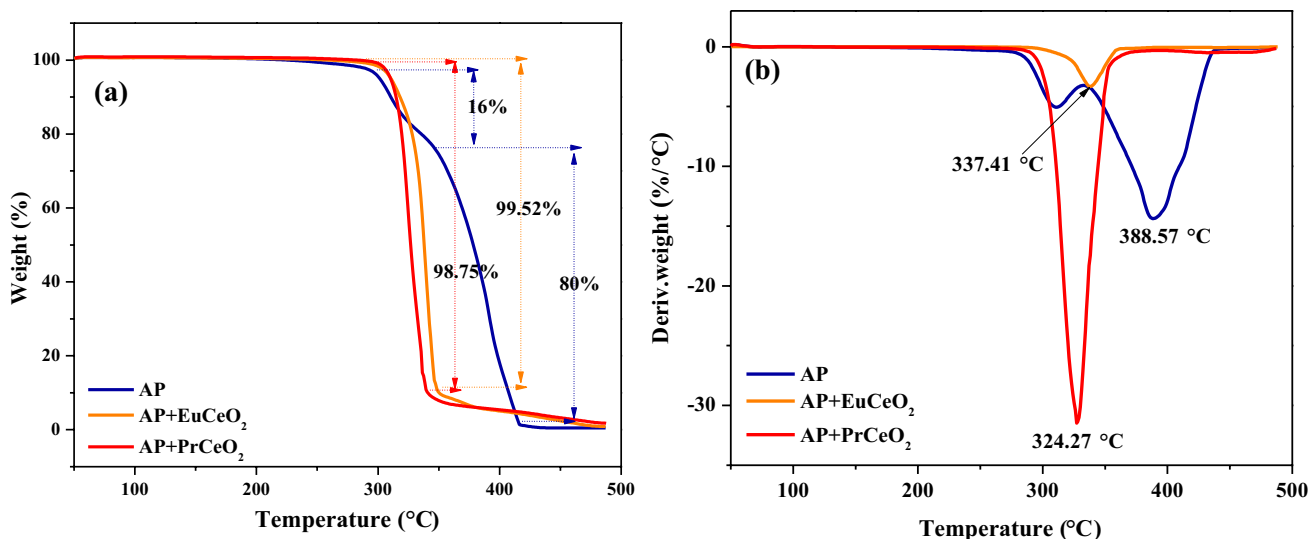


Fig. 4 a TG b DTG thermogram of AP and AP with Eu and Pr doped CeO₂ nanoparticles

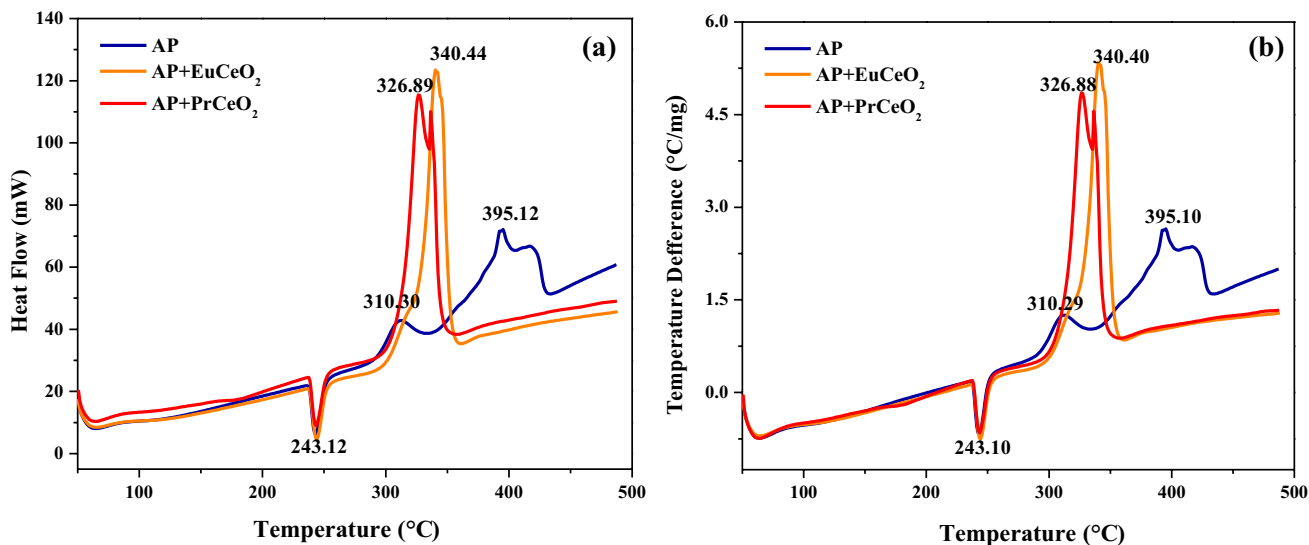


Fig. 5 a DSC b DTA thermogram of AP and AP with Eu and Pr doped CeO₂ nanoparticles

to decompose rapidly at lower temperature. Among the doped nanoparticles, Pr doped CeO₂ nanoparticles exposed excellent catalytic proficiency on the decomposition of AP and decreased the decomposition temperature around 70 °C in contrast to pure AP.

3.3 The catalytic proficiency of nanoparticles on CSPs

The catalytic proficiency of Eu and Pr doped CeO₂ nanoparticles on the thermal decomposition of CSPs were investigated by utilizing the TA Instruments SDT Q600. The Fig. 6 shows the TG curve, it clearly specifies the mass loss

Table 1 Thermal analysis phenomenological data of the AP and AP with Eu and Pr doped CeO₂ nanoparticles (1% by wt.)

Samples	DSC peak (temp. °C)	DTA peak (temp. °C)
AP	310.30 395.12	310.29 395.10
AP + EuCeO ₂	340.44	340.40
AP + PrCeO ₂	326.89	326.88

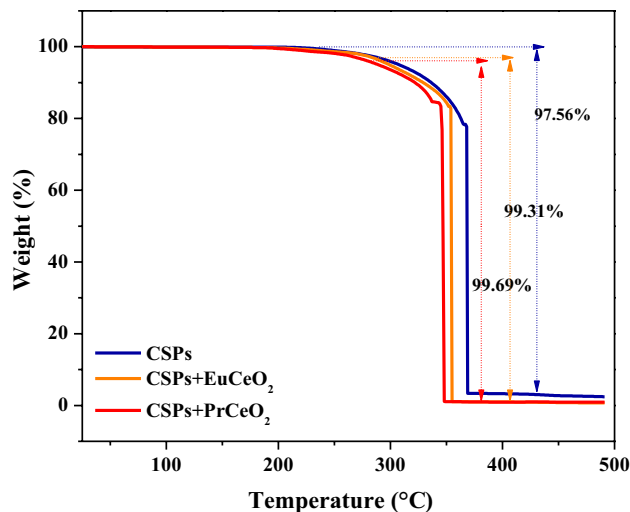


Fig. 6 TG thermogram of AP based CSPs and CSPs with Eu and Pr doped CeO_2 nanoparticles

of CSPs (without nanoparticles) detected at 250–375.43 °C temperature range with 97.56% of mass loss. Further, after incorporation of Eu and Pr doped CeO_2 nanoparticles in the CSPs, TG thermogram clearly stated the decrease in decomposition temperature. The enhancement observed in the mass loss around 99.31% and 99.69% at lower temperature by incorporation of Eu and Pr doped CeO_2 nanoparticles in CSPs. From TG curve, it can be obvious that the Eu and Pr doped CeO_2 nanoparticles are efficient to boost the mass loss of CSPs at a lower temperature.

The DSC results of CSPs with and without Eu and Pr doped CeO_2 nanoparticles are demonstrated in Fig. 7. In the DSC results, it can be found that the decomposition beginning at 240 °C. In the CSPs, AP remains in larger proportion. Therefore, AP led to express of its parent decomposition characteristics. Thus, endothermic AP phase transition peak observed at 243.12 °C for pure AP (Fig. 5a) which shifted to 247.32 °C for CSPs in Fig. 7. The shifting of peak for CSPs owing to the energy is also essential to vaporize the other components in CSPs. The first exothermic peak combine with much stronger second exothermic peak was observed at 370.73 °C characterized by very high heat release. The event signifies the extremely increased exothermicity of CSP over AP that rapid decomposition occurred.

In condensed phase, the exothermic reaction occurs between AP with HTPB. Therefore, the exothermic peak of AP decomposition occurs significantly at a low temperature. In condensed phase reactions of CSPs, the role of AP is the rate-controlling step at least in the temperature range considered in the present study. The decomposition of the CSPs mainly altered by AP due to its present in major proportion in compare to HTPB [54]. In fact, Sell

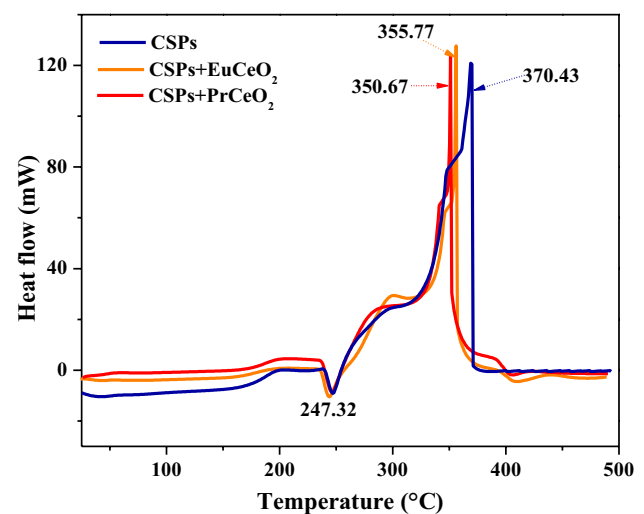


Fig. 7 DSC thermogram of AP based CSPs and CSPs with Eu and Pr doped CeO_2 nanoparticles

et al. showed that it is possible to fully consume AP and majority of HTPB in the temperature range 100–380 °C (weight loss 78%), with just 5% mass loss at higher temperatures attributed to enduring HTPB. Major mass loss in 250–390 °C range concurs with AP. As shown in Fig. 7, the complete decomposition of CSPs occurred with second exothermic peak related to AP. The AP decomposition have tends to release the huge amount of heat.

The shifting of decomposition peak for CSPs at a lower temperature around 370.43 °C is associated with exothermicity of HTPB and AP decomposition which discharge the huge amount of heat and enhance the decomposition rate. The slow preheating of the lower layers of CSPs accompanied by above mentioned response and it also gain the small quantity of heat release as a segment of surface combustion. Overall, the thermal decomposition of HTPB-AP system suggest that the burning rate of the CSPs could improve.

3.3.1 Burning rate of CSPs

The high temperature fascinates the burning of CSPs with sound and fire. The data for burning rates of CSPs with and without Eu and Pr doped CeO_2 nanoparticles (1% by wt.) were originated as 2.22, 3.08, and 3.52 mms^{-1} respectively. The increment in the burning rate associated with enhancement in the condensed phase reactions during combustion of the propellants [55]. In the addition of Eu and Pr doped CeO_2 nanoparticles increased the burning rate of CSPs. In Table 2 clearly observed that Eu and Pr doped CeO_2 nanoparticles increase the burning rate(*r*) of CSPs and it is highest for Pr doped CeO_2 nanoparticles in the CSPs. The Pr doped CeO_2 nanoparticles are efficient

to enhance the burning rate of CSPs around 1.59 times. Among them, Pr doped CeO₂ nanoparticle as considers as the highest enhancer of burning rate than Eu doped CeO₂ nanoparticles.

3.4 Kinetics studies

The kinetic studies of AP and CSPs catalyzed by Eu and Pr doped CeO₂ nanoparticles have been assessed by three different methods viz Flynn–wall–Ozawa (FWO) Kissinger–akahira–sunose (KAS) and Starink methods with different heating rate (5, 10, 15 °C min⁻¹) [31–33]. The plots of $\ln\beta$, $\ln\beta/T^2$ and $\ln\beta/T^{1.92}$ against $1000/T$ of all samples pure AP and CSPs with doped CeO₂ nanoparticles is demonstrated in Fig. 8. From Table 3, it has been calculated that the values activation energies of pure AP are 273.58, 276.23 and 276.47 kJ mol⁻¹ and CSPs activation energies values 249.15, 281.35 and 251.57 kJ mol⁻¹ by FWO, KAS and Starink methods, respectively. After incorporation of Eu and Pr doped CeO₂ nanoparticles, activation energy decreased significantly for AP and CSPs. The results point out that Pr doped CeO₂ nanoparticles has an excellent catalytic proficiency in the increase of rate the decomposition of AP and CSPs. In Table 3, it noticeably displayed the lower in activation energy for AP, CSPs in the occurrence of Eu, and Pr doped CeO₂ nanoparticles. The correlation coefficient (*r*) is nearby to one for graphs. The activation energy is decreased with decreasing the value of exponential factor as the catalytic proficiency increase.

In the DSC based kinetics, activation energy values of Kissinger and Starink methods are similar to each another and are lower than Ozawa method. These parameters could be achieved from the dependence of exothermic peak temperature as a role of heating rate. The Kissinger correlation can be used to define the relationship among decomposition temperature and heating rate [56]. It is known that the Eu and Pr doped CeO₂ nanoparticles have huge surface area because of their very small size and there are many reactive sites over the surface. The promotions of reactions endorsed by Eu and Pr doped CeO₂ nanoparticles by absorbing the gaseous reactive molecules on their surface in the exothermic decomposition.

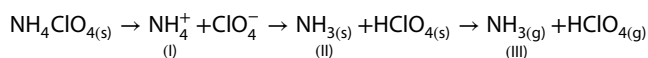
Table 2 Burning rate of CSPs with and without Eu and Pr doped CeO₂ nanoparticles (1% by wt.)

Sample	Burning rate (mm/s)	<i>r</i> */ <i>r</i>
CSPs	2.22	1
CSPs + EuCeO ₂	3.08	1.39
CSPs + PrCeO ₂	3.52	1.59

*r** and *r* are burning rate of CSP with and without Eu and Pr doped CeO₂ nanoparticles, respectively

As results suggests that Pr doped CeO₂ nanoparticles has a greater catalytic proficiency of the decomposition of AP from intermediate products to gaseous products. The activation energy of the decomposition of AP with Pr doped CeO₂ nanoparticles reduce clearly at the ending of reaction, exhibiting unique kinetic parameters of a self-increasing reaction.

The two most significant mechanisms have been reported for the thermal decomposition of AP. In first relies on the electron shift as of perchlorate ion to ammonium ion and second is proton shift as of ammonium ion to perchlorate ion but proton transfer is more acceptable which is as follows [57–63]:



The two most important products ammonia and perchloric acid are identified in the thermal disintegration of AP in previous reports by the researcher [57, 59–63]. The acceptable postulation is that the initial stage of AP decomposition path is proton shift. This mechanism includes three important steps: Step-1 includes a pair of ions in AP lattice. Step-2 includes decay or sublimation step that begins with proton move starting the cation NH₄⁺ to the anion ClO₄⁻, then the molecular complex is formed and decomposes into ammonia and perchloric acid in Step-3. The molecules of ammonia and perchloric acid tend to react in the adsorbed layer on the surface of perchlorate or desorbs and inspiring relating in the gas phase [58].

There is beneficial impact of catalyst on the oxidation of sublimations products of AP decomposition and from Table 3, it can be seen that the activation energy kept low. The reason behind can be illustrated from the understanding of AP decomposition. The decomposition of AP proceeds through a proton transfer and consequent development of ammonia and perchloric acid [64].

The ammonia formation and sublimation phenomena happen in entire process. Further, the magnitude of thermal decomposition of AP impeded by ammonia as well as chlorine that cause downtrend of the reaction. It can be describe by considering the reaction in the adsorbed layer. Where the perchloric acid tends to desorbs more promptly than ammonia and ensues inadequate oxidation of ammonia takes place. Therefore, impregnate environment of ammonia which shelter the crystal surface to interrupt leftover reaction [65, 66]. Such hindrance would consequently desire higher activation energies to precede the reaction and this obliquity noticed in the decomposition of AP [55, 66]. The development of porous AP facilitated in exothermic decomposition and porous AP with higher surface provides floor for adsorption of the gaseous dissociation or decomposition products [66]. The formation of side products likes O₂, N₂O,

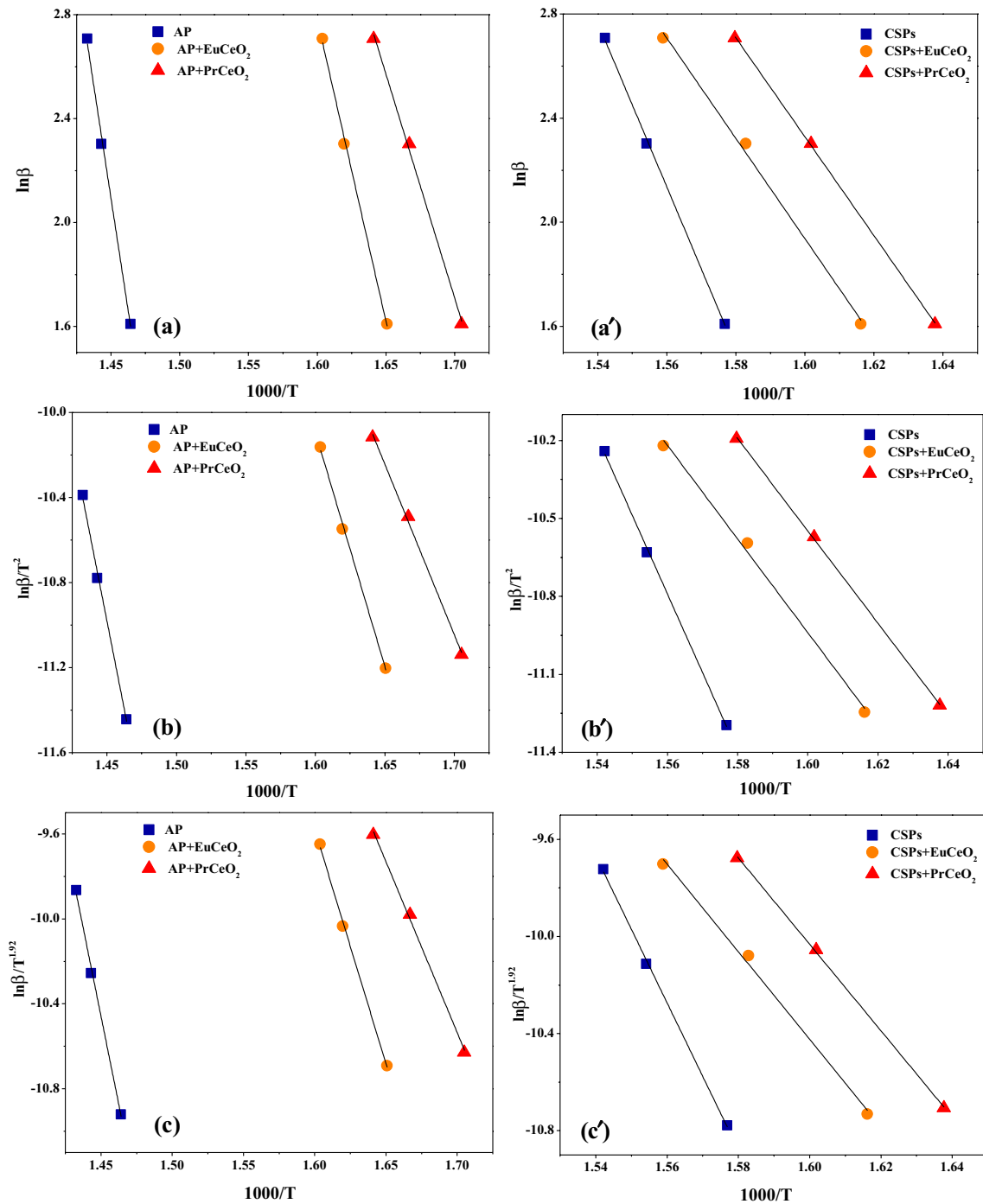


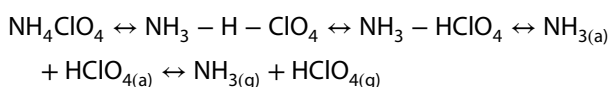
Fig. 8 kinetics plot of **a, b, c** AP and AP with Eu and Pr doped CeO₂ nanoparticles **a', b', c'** AP based CSPs and CSPs with Eu and Pr doped CeO₂ nanoparticles using FWO, KAS and Starink methods

Cl₂, HCl, NO, and H₂O and some less stable species occurred due to multiple reactions between ammonia and perchloric acid [67]. It is highly feasible that these reactions can occur not only in the gas phase, but also in the adsorbed state.

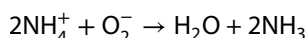
This exert robust deportment in this existing result, the disintegration of perchloric acid will occur in the condensed phase or possibly in the adsorbed state resulting into the development of smaller species (NO, ClO₂, H₂O, N₂O, NO₂ etc.) and which ultimately withdrawals into the gas phase.

Table 3 Thermo-kinetics data of AP, AP with Eu and Pr doped CeO₂ nanoparticles and AP based CSPs, CSPs with Eu and Pr doped CeO₂ nanoparticles using Ozawa, Kissinger and Starink methods

Samples	FWO			KAS			Starink		
	Ea (kJ/mol)	ln A (min ⁻¹)	R ²	Ea (kJ/mol)	ln A (min ⁻¹)	R ²	Ea (kJ/mol)	ln A (min ⁻¹)	R ²
AP	277.58	4.05	0.995	276.23	16.00	0.995	276.47	12.49	0.995
AP + EuCeO ₂	183.73	3.94	0.997	183.07	10.96	0.997	182.03	8.84	0.997
AP + PrCeO ₂	136.26	3.83	0.996	133.42	8.18	0.996	132.75	6.78	0.996
CSPs	252.15	4.04	0.998	251.35	14.70	0.998	251.57	11.57	0.998
CSPs + EuCeO ₂	152.28	3.85	0.993	149.73	9.07	0.992	148.95	7.44	0.992
CSPs + PrCeO ₂	150.12	3.85	0.999	147.60	8.96	0.999	146.83	7.36	0.999

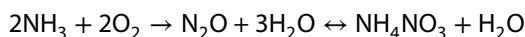
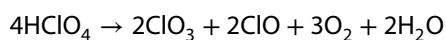
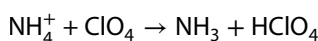
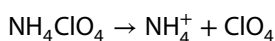


The absorption of gaseous reactive molecule on the surface metal oxide nanoparticles and catalyze the reaction in the proton transfer mechanism noticed. The increment in the thermal decomposition rate of AP is due to the increasing the formation of more holes within the *p*-type semiconducting. The mechanism catalytic efficiency of the catalyst is based on the oxide ion O₂⁻ on the surface of the catalyst. The O₂⁻ formed throughout decomposition of AP and the surface O₂⁻ of catalysts are likely the proton traps during the subsequent reaction [63]:

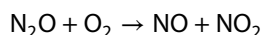
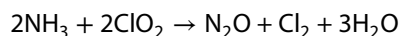
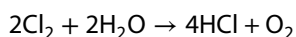
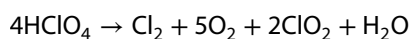


The capacity of O₂⁻ formation and gas absorption on catalyst surface which are the main reasons to completion of AP thermal decomposition. Pr doped CeO₂ nanoparticles surface has produced more O₂⁻ in the contrast of Eu doped CeO₂ nanoparticles. Consequently, it increases the AP decomposition more than Eu doped CeO₂ nanoparticles. The NH₃, H₂O and a minor quantity of N₂O and O₂ are forming during the low-temperature thermal decomposition of AP. While in high-temperature thermal decomposition of AP produces HCl, H₂O, N₂O, NH₃, Cl₂, NO, O₂, NO₂ and a minor quantity of ClO₂.

At low temperature:



At high temperature:



The particles of AP and Eu and Pr doped CeO₂ nanoparticles existing together and expected interaction between the decomposition product and Eu and Pr doped CeO₂ nanoparticles noticed. The hydrogen bonding or coordination types of interaction take place among the ammonia, perchloric acid as well as other decomposition products with doped nanoparticles by the reserved Lewis acid sites. Further interaction may also increase because the disassociate species are captured and not effortlessly liberated into surrounding. The adsorption and interaction types of event generate the intermediates and may endorse the interruption of ammonia as well as the active perchloric acid to smaller species resulting in an alteration in the reaction equilibrium. The faster rate of interruption is associated with surface reaction. Finally, inclusive rate of decomposition will alter which is mainly administrated by the sublimation at these temperatures. Therefore; the possible abstraction of dissociation products at a faster rate would inspire the dissociation of AP. Hence, this catalytic interaction and consequent equilibrium change as expected may have elicited in the lowering of Ea values for the catalyzed decomposition. Also activation energy may be interrelated to bond energy data [68] and is generally considered as a measurement of the energy obstacle to a regulating (rate limiting) bond split or bond redistribution step [69]. The lowering of activation energy values depends on the generation of oxidizing species with low bond enthalpies. Therefore, interaction of doped Eu and Pr doped nanoparticles with such species contributed to lowering of activation energies.

4 Conclusion

The Eu and Pr doped CeO₂ nanoparticles were synthesis through chemical co-precipitation process. The catalytic impact of Eu and Pr doped CeO₂ nanoparticles were evaluated using TG–DSC techniques. The thermal decomposition temperature of AP has decreased due to the catalyst, it was reduced around 70 °C and it is fast decomposition of AP at lower temperature. Pr doped CeO₂ nanoparticle was more efficient than others and the thermal decomposition temperature of AP based CSPs shifts descending around 20 °C and burning rate of CSPs was also increased by addition nanoparticles. The activation energy decreased with decreasing the value of exponential factor (A) as the catalytic activity increases. Pr doped CeO₂ nanoparticle is a good catalyst than Eu doped CeO₂ nanoparticle in the CSPs.

Acknowledgements The authors are grateful to the Department of Chemistry, K S KV Kachch University, Bhuj for laboratory facility and for XRD, SEM and TGA–DSC analysis and also thankful to Chemistry Department, Sardar Patel University, Vallabh Vidyanagar for providing ATR-FTIR instrument facility.

Compliance with ethical standards

Conflict of interest The authors declare that they have no conflict of interest.

Research involving human participants and/or animals Not applicable.

References

- Nzungung VA, Wang CH, Harvey G (1999) Plant-mediated transformation of perchlorate into chloride. *Environ Sci Technol* 33:1470–1478
- Ulas A, Risha GA, Kuo KK (2006) Ballistic properties and burning behaviour of an ammonium perchlorate/guanidine nitrate/sodium nitrate airbag solid propellant. *Fuel* 85:1979–1986
- Yang RJ, Gao DY, Huang H, Huang B, Cai HQ (2013) Mesoporous silicas prepared by ammonium perchlorate oxidation and their application in the selective adsorption of high explosives. *Microporous Mesoporous Mater* 168:46–50
- Lewis WK, Harruff BA, Gord JR, Rosenberger AT, Sexton TM, Guliants EA, Bunker CE (2011) Chemical dynamics of aluminum nanoparticles in ammonium nitrate and ammonium perchlorate matrices: enhanced reactivity of organically capped aluminum. *J Phys Chem C* 115:70–77
- Ajaz AG (1995) Estimation of ammonium perchlorate in HTPB based solid propellants using Kjeldahl method. *J Hazard Mater* 42:303–306
- Hedman TD, Reese DA, Cho KY, Groven LJ, Lucht RP, Son SF (2012) An experimental study of the effects of catalysts on an ammonium perchlorate based composite propellant using 5 kHz PLIF. *Combust Flame* 159:1748–1758
- Hedman TD, Groven LJ, Cho KY, Lucht RP, Son SE (2013) The diffusion flame structure of an ammonium perchlorate based composite propellant at elevated pressures. *Proc Combust Inst* 34:649–656
- Fitzgerald RP, Brewster MQ (2004) Flame and surface structure of laminate propellants with coarse and fine ammonium perchlorate. *Combust Flame* 136:313–326
- Zepf V (2016) An overview of the usefulness and strategic value of rare earth metals A2—Lima, Ismar Borges De. In: Filho WL (ed) *Rare earths industry*. Elsevier, Boston, pp 3–17 (**Chapter 1**)
- Du X, Graedel TE (2011) Global in-use stocks of the rare earth elements: a first estimate. *Environ Sci Technol* 45:4096–4101
- Chakhmouradian AR, Wall F (2012) Rare earth elements: minerals, mines, magnets (and more). *Elements* 8:333–340
- Singh P, Mahadevaiah N, Parida SK, Hegde MS (2011) Ru⁴⁺ ion in CeO₂ (Ce_{0.95}Ru_{0.05}O₂–δ)–δ): a non-deactivating, non-platinum catalyst for water gas shift reaction. *J Chem Sci* 123(5):577–592
- Xiao G, Li S, Li H, Chen L (2009) Synthesis of doped ceria with mesoporous flowerlike morphology and its catalytic performance for CO oxidation. *Microporous Mesoporous Mater* 120:426–431
- Vanpoucke DEP, Bultinck P, Cottenier S, Speybroeck VV, Driessche IV (2014) Aliovalent doping of CeO₂: DFT study of oxidation state and vacancy effects. *J Mater Chem A* 2:13723–13737
- Vanpoucke DEP, Cottenier S, Speybroeck VV, Driessche IV, Bultinck P (2014) Tetravalent doping of CeO₂: the impact of valence electron character on group IV dopant influence. *J Am Ceram Soc* 97(1):258–266
- Jampaiah D, Tur KM, Ippolito SJ, Sabri YM, Tardio J, Bhargava SK, Reddy BM (2013) Structural characterization and catalytic evaluation of transition and rare earth metal doped ceria-based solid solutions for elemental mercury oxidation. *RSC Adv* 3:12963–12974
- Yang Z, Woo TK, Hermansson K (2006) Oxygen vacancy formation and migration in Ce_{1-x}Zr_xO₂/Ce_{1-x}Zr_xO₂ catalyst: a DFT+UDFT+U calculation. *J Chem Phys* 124:224704
- Widmann D, Leppelt R, Behm RJ (2007) Activation of a Au/CeO₂ catalyst for the CO oxidation reaction by surface oxygen removal/oxygen vacancy formation. *J Catal* 251:437–442
- Lanje AS, Ningthoujam RS, Shrama SJ, Vatsa RK, Ponde RB (2010) Luminescence properties of Sn_{1-x}FexO₂ nanoparticles. *Int J Nanotechnol* 7:979–988
- Wolffarth EP (1980) *Ferromagnetic materials*. North-Holland, Amsterdam, New York, Oxford, Tokyo, p 2
- Mitsuyu T, Yamakazi O, Ohji K, Wasa K (1982) Piezoelectric thin films of zinc oxide for saw devices. *Ferroelectrics* 42:233–240
- Regan O, Gratzel M (1991) A low-cost, high-efficiency solar cell based on dye-sensitized colloidal TiO₂ films. *Nature* 353:737–740
- Jacobs PWM, Whitehead HM (1969) Decomposition and combustion of ammonium perchlorate. *Chem Rev* 69(4):551–590
- Jain SR, Nambiar PR (1976) Effect of tetra methyl ammonium perchlorate on ammonium perchlorate and propellant decomposition. *Thermochim Acta* 16(1):49–54
- Ma ZY, Li FS, Bai HP (2006) Effect of Fe₂O₃ in Fe₂O₃/AP composite particles on thermal decomposition of AP and on burning rate of the composite propellant. *Propell Explos Pyrotech* 31(6):447–451
- Wang Y, Yang X, Lu L, Wang X (2006) Experimental study on preparation of LaMO₃ (M=Fe Co, Ni) nanocrystals and their catalytic activity. *Thermochim Acta* 443(2):225–230
- Singh G, Kapoor IPS, Dubey S, Siril PF, Hua YJ, Zhao FQ, Hu RZ (2008) Effect of mixed ternary transition metal ferrite nanocrystallites on thermal decomposition of ammonium perchlorate. *Thermochem Acta* 477:42–47
- Birks LS, Friedman H (1946) Particle size determination from X-Ray line broadening. *J Appl Phys* 17(8):687–692
- Krishna S, Swami RD (1997) Effect of catalyst mixing procedure on subatmospheric combustion characteristics of composite propellants. *J Propul Power* 13:207–212

30. Singh G, Kapoor IPS, Dubey S (2009) Bimetallic nanoalloys: preparation, characterization and their catalytic activity. *J Alloys Compd* 480:270–274
31. Cheng Y, Li Y, Yan S, Huang C (2010) Deviation of activation energy caused by neglecting a temperature term in Ozawa Equation. *J Math Chem* 48:704–713
32. Chen T, Du P, Jiang W, Liu J, Hao G, Gao H, Xiao L, Ke X, Zhao F, Xuan C (2016) A facile one-pot solvothermal synthesis of $\text{CoFe}_2\text{O}_4/\text{RGO}$ and its excellent catalytic activity on thermal decomposition of ammonium perchlorate. *RSC Adv* 6:83838–88347
33. Starink MJ (2003) The determination of activation energy from linear heating rate experiments: a comparison of the accuracy of isoconversion methods. *Thermochim Acta* 404:163–176
34. Liu X, Chen S, Wang X (2007) Synthesis and photoluminescence of $\text{CeO}_2:\text{Eu}^{3+}$ phosphor powders. *J Lumin* 127:650–654
35. Sahoo SK, Mohapatra M, Anand S (2013) Characterization and optical properties of Eu-doped cubic nano ceria synthesized by using the co-precipitation-hydrothermal route. *J Korean Phys Soc* 62(2):297–304
36. Khan MAM, Khan W, Ahamed M, Alhazaa AN (2017) Microstructural properties and enhanced photocatalytic performance of Zn doped CeO_2 nanocrystals. *Sci Rep* 7(1):12560 1–11
37. Vinothkumar G, Amalraj R, Babu KS (2017) Fuel-oxidizer ratio tuned luminescence properties of combustion synthesized europium doped cerium oxide nanoparticles and its effect on antioxidant properties. *Ceram Int* 43(7):5457–5466
38. Rodrigues MA, Catto AC, Longo E, Nossol E, Lima RC (2018) Characterization and electrochemical performance of CeO_2 and Eu-doped CeO_2 films as a manganese redox flow battery component. *J Rare Earths* 36(10):1074–1083
39. Bharathi RN, Sankar S (2018) Structural, optical and magnetic properties of Pr doped CeO_2 nanoparticles synthesized by citrate–nitrate auto combustion method. *J Mater Sci Mater Electron* 29:6679–6691
40. Samiee S, Goharshadi EK (2012) Effects of different precursors on size and optical properties of ceria nanoparticles prepared by microwave- assisted method. *Mater Res Bull* 47:1089–1095
41. Wang G, Mu Q, Chen T, Wang Y (2010) Synthesis, characterization and photoluminescence of CeO_2 nanoparticles by a facile method at room temperature. *J Alloy Compd* 493:202–207
42. Ho C, Yu JC, Kwong T, Mak AC, Lai S (2005) Morphology-controllable synthesis of mesoporous CeO_2 nano- and microstructures. *Chem Mater* 17:4514–4522
43. Tholkappiyar R, Vishista K (2014) Synthesis and characterization of barium zinc ferrite nanoparticles: working electrode for dye sensitized solar cell applications. *Sol Energy* 106:118–128
44. Sajjada M, Ullaha I, Khan MI, Khan J, Khan MY, Qureshid MT (2018) Structural and optical properties of pure and copper doped zinc oxide nanoparticles. *Results Phys* 9:1301–1309
45. Jacobs PMW, Parosone GS (1969) Mechanism of the decomposition of ammonium perchlorate. *Combust Flame* 13:419–425
46. Rosser WA, Inami SH (1968) Thermal decomposition of ammonium perchlorate. *Combust Flame* 12:427–435
47. Kishore K, Sridhara K (1990) Solid propellant chemistry: condensed phase behaviour of ammonium perchlorate based solid propellants. DESIDOC, New Delhi, p 10
48. Padwal MB, Varma M (2018) Thermal decomposition and combustion characteristics of HTPB-coarse AP composite solid propellants catalyzed with Fe_2O_3 . *Combust Sci Technol* 190(9):1614–1629
49. Zhi J, Feng-Qi Z (2002) Study on effects of nanometer metal powder on thermal decomposition of HMX. *J Propul Technol* 23:258–261
50. Al-Harathi A, Williams A (1998) Effect of fuel binder and oxidizer particle diameter on the combustion of ammonium perchlorate based propellants. *Fuel* 77:1451–1468
51. Ishitha K, Ramakrishna PA (2014) Studies on the role of iron oxide and copper chromite in solid propellant combustion. *Combust Flame* 161(10):2717–2728
52. Vyazovkin S, Wight CA (1998) Isothermal and non-isothermal kinetics of thermally stimulated reactions of solids. *Int Rev Phys Chem* 17(3):407–433
53. Vyazovkin S, Wight CA (1999) Kinetics of thermal decomposition of cubic ammonium perchlorate. *Chem Mater* 11:3386–3393
54. Sell T, Vyazovkin S, Wight CA (1999) Thermal decomposition kinetics of PBAN-binder and composite solid rocket propellants. *Combust Flame* 119(1):174–181
55. Singh G, Kapoor IPS, Pandey DK (2002) Hexamine metal perchlorates as energetic burning rate modifiers. *J Energy Mater* 20:223–244
56. Burnhamb AK, Vyazovkin S, Criadoc JM, Perez-Maquedac LA, Popescud C, Sbirrazzuolie N (2011) ICTAC Kinetics Committee recommendations for performing kinetic computations on thermal analysis data. *Thermochim Acta* 520:1–19
57. Joshi SS, Patil PR, Krishnamurthy VN (2008) Thermal decomposition of ammonium perchlorate in the present of nanosized ferric oxide. *Def Sci J* 58:721–727
58. Zhao S, Ma D (2010) Preparation of CoFe_2O_4 nanocrystallites by solvothermal process and its catalytic activity on the thermal decomposition of ammonium perchlorate. *J Nanomater* 2010:1–5
59. Wang Y, Xia X, Zhu J, Li Y, Wang X, Hu X (2011) Catalytic activity of nanometer-sized $\text{CuO}/\text{Fe}_2\text{O}_3$ on thermal decomposition of AP and combustion of AP-based propellant. *Combust Sci Technol* 183:154–162
60. Singh G, Kapoor IPS, Dubey S, Siril PF (2009) Preparation, characterization and catalytic activity of transition metal oxide nanocrystals. *J Sci Conf Proc* 1:11–17
61. Liu T, Wang L, Yang P, Hu B (2008) Preparation of nanometer CuFe_2O_4 by auto-combustion and its catalytic activity on the thermal decomposition of ammonium perchlorate. *Mater Lett* 62:4056–4058
62. Xu H, Wang X, Zhang L (2008) Selective preparation of nanorods and micro-octahedrons of Fe_2O_3 and their catalytic performances for thermal decomposition of ammonium perchlorate. *Powder Technol* 185:176–180
63. Li L, Sun X, Qiu X, Xu J, Li G (2008) Nature of catalytic activities of CoO nanocrystals in thermal decomposition of ammonium perchlorate. *Inorg Chem* 47:8839–8846
64. Heath GA, Majer JR (1964) Mass spectrometric study of the thermal decomposition of ammonium perchlorate. *Trans Faraday Soc* 60:1783–1791
65. Boldyrev VV (2006) Thermal decomposition of ammonium perchlorate. *Thermochim Acta* 443:1–36
66. Jacobs PWM, Russell-Jones A (1968) Sublimation of ammonium perchlorate. *J Phys Chem* 72:202–207
67. Mallick L, Kumar S, Chowdhury A (2015) Thermal decomposition of ammonium perchlorate—a TGA–FTIR–MS study: part I. *Thermochim Acta* 610:57–68
68. Schmid R, Sapunov VN (1982) Non-formal kinetics: in search of chemical reaction pathways. Verlag Chemie GmbH, Weinheim
69. Galwey AK (2004) Is the science of thermal analysis kinetics based on solid foundations? A literature appraisal. *Thermochim Acta* 413:139–183

Publisher's Note Springer Nature remains neutral with regard to jurisdictional claims in published maps and institutional affiliations.